

Nanostructured Cellular Networks

P. Moriarty and M. D. R. Taylor

School of Physics and Astronomy, University of Nottingham, Nottingham NG7 2RD, United Kingdom

M. Brust

*Centre for Nanoscale Science, Department of Chemistry, University of Liverpool,
Crown Street, Liverpool L69 7ZD, United Kingdom*

(Received 28 March 2002; published 25 November 2002)

Au nanocrystals spin-coated onto silicon from toluene form cellular networks. A quantitative statistical crystallography analysis shows that intercellular correlations drive the networks far from statistical equilibrium. Spin-coating from hexane does not produce cellular structure, yet a strong correlation is retained in the positions of nanocrystal aggregates. Mechanisms based on Marangoni convection alone cannot account for the variety of patterns observed, and we argue that spinodal decomposition plays an important role in foam formation.

DOI: 10.1103/PhysRevLett.89.248303

PACS numbers: 61.46.+w, 82.70.Rr

Random cellular networks are ubiquitous in nature. Soap froths, metallurgical grains, geological artifacts, biological tissues, and even the galactic-scale structure of the Universe all exhibit similar cellular characteristics despite the disorder inherent in each system and the vast differences in length scales [1]. That this structural similarity is observed for a variety of networks having radically different formation mechanisms hints strongly at an underlying universal behavior. Statistical crystallography [2] is derived from the fundamental postulate underlying this universality and enables quantifiable characterization of a cellular network.

Here we report that, under appropriate conditions, Au nanocrystals on silicon also form cellular networks. Although polygonal nets of nanoparticles have recently been observed [3,4], there has been no attempt to date to determine what parallels exist between nanocrystal networks and the cellular systems listed above. Using statistical crystallography, we not only show that nanostructured foams are structurally distinct from a variety of prototypical froths but also conclusively demonstrate that mechanisms based solely on Marangoni convection [3,4] fail to explain many aspects of cellular network formation in nanocrystal systems.

Thiol ($C_5H_{11}S$)-passivated Au nanocrystals of 2 nm core diameter were prepared via the method of Brust *et al.* [5] and dispersed in either a toluene or a hexane solvent. Nanocrystal concentrations ranging between 2.5×10^{-2} and 0.101 g/l were used for both the toluene and the hexane dispersions. 10 μ l of the nanocrystal solution was spin-coated onto a 1 cm² native-oxide covered Si(111) sample for 30 sec at a rotation speed of 4 krpm [6]. Tapping mode atomic force microscopy (TM-AFM) was carried out using a Digital Instruments D3100.

Figure 1 shows the morphology of typical nanocrystal submonolayers formed when toluene is used as the sol-

vent. These overlayers are best described as random cellular networks [1,2] and line sections through the networks show that they are a single nanocrystal thick. Although Fig. 1(a) at first glance is similar to recent transmission electron microscopy images of polygonal nanocrystal networks [3,4], there is a key difference. From higher magnification images [e.g., Fig. 1(b)], it is

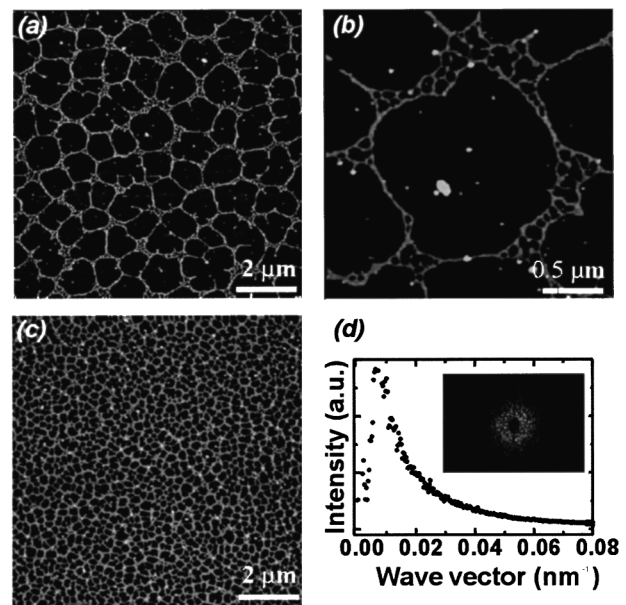


FIG. 1. (a) TM-AFM image of typical foam (13% areal coverage, 2.5×10^{-2} g/l nanocrystal concentration) resulting from spin-coating C_5 -thiol passivated 2-nm diameter Au nanocrystals onto a native oxide-covered Si substrate at 4 krpm; (b) a higher magnification image of the fine structure of the nanocrystal network shown in (a). (c) As (a), except 33% coverage (concentration: 0.101 g/l); (d) radially averaged FFT of $20 \times 20 \mu\text{m}^2$ image taken in the vicinity of the region shown in (a). Inset shows corresponding 2D FFT.

clear that at the junctions of the larger polygons there exist secondary, minor networks. Furthermore, when the nanocrystal concentration in solution is increased, the separation of the network cells *decreases*. Both the observation of coexisting networks with strongly differing intercell separations *and* the reduction in intercellular spacing for increasing nanocrystal concentration have important implications for theories of network formation based solely on Marangoni convection. We discuss this in detail below.

It is clear that the submonolayers shown in Fig. 1 are not long-range ordered. However, a reciprocal space analysis shows that there *is* a preferred intercellular separation. The inset in Fig. 1(d) is a 2D fast Fourier transform (FFT) which yields the structure factor for the (primary) network. While no spots are observed in the structure factor, highlighting a lack of orientational order, a ring with a radius of $\sim 0.007 \text{ nm}^{-1}$ is visible. A radial average of the FFT [Fig. 1(d)] emphasizes this peak in wave-vector space. The network is thus associated with a well-defined intercellular correlation length which is concentration-dependent [compare Figs. 1(a) and 1(c)].

A more detailed structural analysis is possible using statistical crystallography [1,2]. Figure 2(c) is the Voronoi construction [1,2] for a network image acquired from the same sample as shown in Fig. 1(c) [8]. The associated probability distribution of polygon sidedness is shown in Fig. 2(a). There are a number of important parameters that may be measured directly from this histogram. First, the mean number of polygon sides $\langle n \rangle$ for all nanocrystal networks we have studied is ≥ 5.98 . This is extremely close to the value of 6 expected in the limit of an infinite network [1,2] and indicates that our data are not statistically skewed through insufficient sampling. Cells with less than four or greater than nine sides are not observed and when nine-sided cells are present their number is very small ($\sim 1\%$).

The polygon distribution shown in Fig. 2(a) is both unimodal and has a very low second moment, $\mu_2 = \sum p(n)(n - \langle n \rangle)^2$. While low μ_2 values are generally

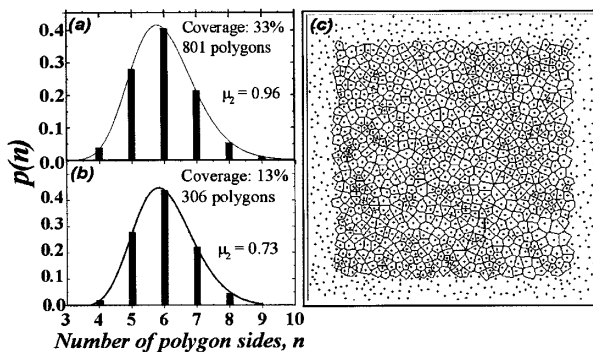


FIG. 2. Histograms of polygon side distributions for (a) 33% coverage, (b) 13% coverage. The solid curves are log-normal [7] fits to the distributions. (c) A typical Voronoi tessellation for a 33% coverage nanocrystal foam.

associated with young systems that are far from statistical equilibrium, we note that even the prototypical quenched froth, the 2D Poisson Voronoi tessellation, has a significantly larger value of μ_2 (1.78 [9]) than that observed for the nanocrystal network. That the networks shown in Fig. 1 are not derived from a Poisson distribution of points, and thus do not arise from nucleation or dewetting events that are spatially uncorrelated [10], may also be quantifiably confirmed from a measure of their entropy, $S = -\sum_n P_n \ln P_n$. For all nanocrystal foams we have studied, S is 1.40 ± 0.05 , substantially smaller than the value of 1.71 expected for a purely random 2D set of points [9]. An analysis of Voronoi constructions taken from a number of regions neighboring that shown in Fig. 1(a) resulted in the histogram shown in Fig. 2(b). The variance value in this case is substantially lower (0.73) than that observed for networks synthesized from higher concentration solutions ($\mu_2 \sim 1$).

There are a number of topological correlations associated with cellular systems. Foremost among these is the Aboav-Weaire law [1,2] which posits that the product of a cell's sidedness, n , and its neighbors' average sidedness, m , is linear in n :

$$m(n) = (6 - a) + (6a + \mu_2)/n, \quad (1)$$

where μ_2 is again the variance and a is a network parameter. In Fig. 3(a) the linear dependence of $m(n)$ on $1/n$ is clear [11], with the slope and intercept giving consistent values for μ_2 and a for each nanocrystal network. The value of $m(6)$ is independent of a [7] and is given by the Weaire relationship, $m(6) = \langle n \rangle + \mu_2/6$.

The $m(n)$ vs $1/n$ data for each network superimpose—the value of a , 1.0 ± 0.1 , is essentially coverage independent. Significantly, in networks which evolve via cell division or cell disappearance [11–13], a is approximately unity. The observation that each plot in Fig. 3(a) conforms to the Aboav-Weaire law with $a \sim 1$ suggests that topological transformations similar to those occurring in biological and polycrystal systems may underlie the evolution of nanocrystal networks. However, we reiterate that the low variance value is indicative of a system far from statistical equilibrium.

Originally empirically derived from a study of biological cells [14], Lewis's law—which states that the average area of an n -sided cell increases linearly with n —was subsequently shown to represent an equation of state of an ideal cellular network [2,15]. This is an exceptionally powerful deduction, as perfect agreement with Lewis's law then implies that a cellular network's structure is determined *solely* by the mathematics of space filling. Deviations from Lewis's law [1,11,13] indicate that physical forces in addition to topological constraints must be considered. We find that (within fairly large error bars due to the “natural spread” in polygon areas) a quadratic rather than linear relationship provides a better fit to the polygon average area data [Fig. 3(b)]. Although

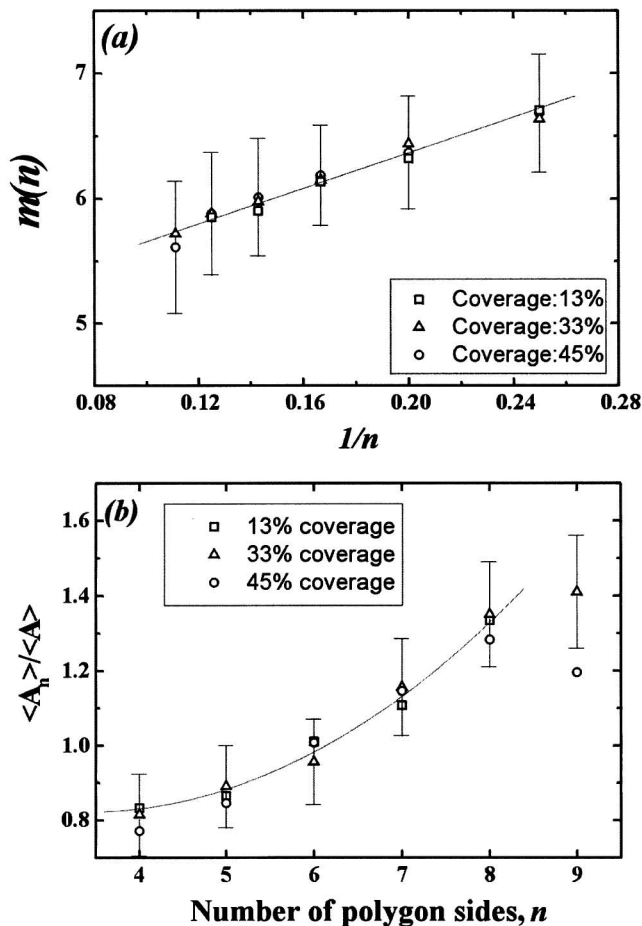


FIG. 3. (a) Plot of $m(n)$, the average number of sides of the neighbors of an n -sided polygon, vs $1/n$ for various nanocrystal coverages. The linear dependence of $m(n)$ on $1/n$ indicates that the Aboav-Weaire law holds (the slope and intercept are 7.0 ± 0.6 and 4.9 ± 0.1 , respectively). (b) Plot of the normalized average area of an n -sided polygon vs n (Lewis' law). A quadratic curve provides a higher correlation coefficient for the fit than a linear relationship (0.991 as compared to 0.969). The fit is based on the average area values for four- to eight-sided polygons (the points for nine-sided polygons are derived from $\sim 1\%$ of the data set). In both (a) and (b) for clarity the error bars are shown only for a single coverage and represent 1 standard deviation. Error bars for all coverages are similar.

the error bars unfortunately prevent definitive conclusions regarding Lewis's law to be reached, we note that, given the far from (statistical) equilibrium state of the nanocrystal cellular system, deviations from the Lewis relation are not unexpected [2]. This contrasts strongly with the statistical crystallography of systems such as biological cells [1,14] and Benard-Marangoni convection patterns [16].

That nanocrystal cellular networks may be structurally distinct from Benard-Marangoni convection patterns has an interesting bearing on our results. The Marangoni effect has recently been proposed as the basis for the formation of nanoparticle networks [3,4]. Marangoni convection alone cannot account for the wide variety of

nanocrystal foams we observe for the following reasons. First, the Marangoni effect is associated with a well-defined instability wavelength λ , given by $\lambda = (2\pi d\sqrt{8})/\sqrt{M_a}$, where d is the fluid layer thickness and M_a is the Marangoni number [17]. The coexistence of cellular networks with radically different intercellular spacings, as seen in Figs. 1(a) and 1(b), is incompatible with *both* networks having arisen from Marangoni convection. To clarify, while we concur with other studies [3,4] that the Marangoni effect is the most plausible mechanism underlying the formation of the major network observed in Fig. 1(a), it completely fails to account for the coexistence of the minor (shorter wavelength) network observed most clearly in Fig. 1(b). Second, Stowell and Korgel [4] have carried out a careful study of the dependence of the Marangoni number on nanocrystal concentration. They find that M_a scales *inversely* with nanocrystal concentration. Thus, the instability wavelength (i.e., intercellular spacing) should lengthen as the nanocrystal concentration is increased. Precisely the opposite is observed in Fig. 1.

The foams discussed thus far result from spin-coating of nanocrystals from *toluene*. Spin-coating of a solution of nanocrystals in hexane does not produce cellular networks. Following Maillard *et al.* [3], it is possible to show that the Marangoni number for hexane is significantly larger than that for toluene [due primarily to vapor pressure differences: $P_{vp}(\text{hexane}) \sim 4P_{vp}(\text{toluene})$ at 300 K]. Thus, the probability of establishing a supercritical Marangoni number is much greater for hexane. Despite this, cellular networks do not form. Instead, for condensation from hexane structures ranging from isolated "droplets" to labyrinthine patterns [Figs. 4(a) and 4(b)] are observed. These patterns bear a striking qualitative similarity to those produced via spinodal phase separation [18].

A particular signature of the early stages of a spinodal process is the presence of spatially correlated aggregates [18,19]. Thiele *et al.* [20] have used pair correlation functions to identify spatially correlated centers arising from spinodal dewetting. An alternative approach is to construct a Voronoi tessellation based on the mass centers of the aggregates and calculate its entropy. A Voronoi tessellation (not shown) for Fig. 4(a) yields $S = 1.39$, again

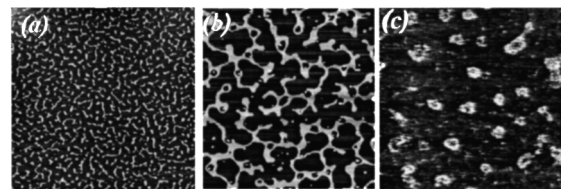


FIG. 4. (a),(b) Examples of spinodal decomposition patterns resulting from spin-coating of C_5 thiol-passivated 2 nm diameter Au nanocrystals from hexane. Image sizes and nanocrystal concentrations: $10 \times 10 \mu\text{m}^2$, $2.5 \times 10^{-2} \text{ g/l}$ and $5 \times 5 \mu\text{m}^2$, 0.101 g/l , respectively. (c) TM-AFM image ($20 \times 20 \mu\text{m}^2$) taken under nanocrystal/toluene solution.

significantly lower than that expected for a Poisson distribution of points [but remarkably similar to the value obtained for Fig. 1(c)]. Hence, it appears that, for condensation from both hexane and toluene, nanocrystal overlayers comprise strongly spatially correlated aggregates. *The presence of a preferred wavelength will tend to drive the system away from statistical equilibrium*, narrowing the polygon side distribution and thus explaining the low values of μ_2 we observe.

Having rejected Marangoni convection as the formation mechanism for the shorter wavelength networks seen in Figs. 1(b) and 1(c), yet requiring that a preferred length scale is accentuated during overlayer assembly, a spinodal process [19] is the most plausible alternative. We first consider spinodal dewetting. Using Lifshitz theory [21] we have calculated the Hamaker constants for C₅-thiol capped Au nanoclusters of 2 nm diameter interacting—via a solvent medium—with a SiO₂ or a Si substrate. Although the interparticle interaction energies in the solvent (~ 15 meV) are comparable to those for the nanoparticle-solvent-SiO₂ systems, initially suggesting that dewetting processes may play a role, we stress three points. First, as the substrate used in our studies is a native oxide-covered Si sample, the true interaction energy will lie somewhere between the nanoparticle-Si value (which we estimate as ~ -200 meV) and that for SiO₂ and will, thus, always be < 0 . Second, similar nanocrystal arrangements form on silicon substrates whose native-oxide layer had been removed via HF etching. In that case, there is unambiguous complete wetting and there is no contribution to the effective Hamaker constant which could engender a spinodal *dewetting* process [22]. Finally, the AFM images lack the height modulations expected for spinodal dewetting: each overlayer is a single nanocrystal thick.

Although the nanoparticle arrangements we observe therefore most likely arise via spinodal decomposition, there is a key difference with the spinodal mechanism postulated by Ge and Brus [19]. This is illustrated in Fig. 4(c), an image taken *under* a toluene-nanocrystal solution where it is clear that nanocrystal islands have nucleated. Figure 4(c) (and work by Lin *et al.* [23]) illustrates that for Au nanocrystals both spinodal and conventional nucleation pathways may contribute in establishing an overlayer morphology. Furthermore, Tanaka [18] has carried out a detailed theoretical study of viscoelastic phase separation in binary systems. Particularly in the latter stages of solvent evaporation where the effective viscosity of the nanocrystal fluid will dramatically increase, we postulate that viscoelastic phase separation provides an alternative explanation to that put forward in Ref. [19] for the observation of nanocrystal spinodal patterns.

In summary, we have shown that Au nanocrystals form cellular networks on silicon surfaces and that Marangoni

convection alone cannot explain the various foams and patterns we observe. Nanocrystal foams are far from statistical equilibrium due to the imposition of a specific intercellular wavelength that dominates network evolution.

We acknowledge financial support from the U.K. Engineering and Physical Sciences Research Council (EPSRC) and thank John Boland, Alex Shard, Peter Coles, and David Schiffrin for helpful discussion. M. B. acknowledges support from EPSRC.

-
- [1] D. Weaire and N. Rivier, *Contemp. Phys.* **25**, 59 (1984).
 - [2] N. Rivier, *Philos. Mag. B* **52**, 795 (1985).
 - [3] M. Maillard *et al.*, *J. Phys. Chem. B* **104**, 11871 (2000).
 - [4] C. Stowell and B. A. Korgel, *Nano Lett.* **1**, 595 (2001).
 - [5] M. Brust *et al.*, *J. Chem. Soc. Chem. Commun.* **7**, 801 (1994).
 - [6] Varying the spin speed between 2 and 8 krpm (for a given nanocrystal concentration) did not change the nanocrystal patterns observed. See D. E. Haas and D. P. Birnie, *J. Mater. Sci.* **37**, 2109 (2002) for a discussion of the effects of rotation speed in spin-coating.
 - [7] D. Weaire, *Metallography* **7**, 157 (1974). We find that gamma fits [see, for example, H. X. Zhu, S. M. Thorpe, and A. H. Windle, *Philos. Mag. A* **81**, 2765 (2001)] do not systematically yield lower χ^2 values than log-normal fits.
 - [8] The coordinates of the cell centers are passed to the QHull utility [C. B. Barber *et al.*, *ACM Trans. Math. Softw.* (1996); <http://www.geom.umn.edu/locate/qhull>] which returns the vertices of the polygons comprising the Voronoi tessellation.
 - [9] S. Kumar and S. K. Kurtz, *Mater. Charact.* **31**, 55 (1993).
 - [10] P. C. Ohara and W. M. Gelbart, *Langmuir* **14**, 3418 (1998).
 - [11] J. C. Earnshaw and D. J. Robinson, *Phys. Rev. Lett.* **72**, 3682 (1994).
 - [12] J. C. Mombach *et al.*, *J. Phys. D* **23**, 600 (1990).
 - [13] D. A. Aboav, *Metallography* **3**, 383 (1970).
 - [14] F. T. Lewis, *Anat. Rec.* **38**, 341 (1928).
 - [15] N. Rivier and A. Lissowski, *J. Phys. A* **15**, L143 (1982).
 - [16] P. Cerisier, S. Rahal, and N. Rivier, *Phys. Rev. E* **54**, 5086 (1996).
 - [17] H. Benard, *Rev. Gen. Sci. Pures Appl. Bull. Assoc. Fr. Av. Sci.* **11**, 1261 (1900); J. R. A. Pearson, *J. Fluid Mech.* **4**, 489 (1958).
 - [18] H. Tanaka, *J. Phys. Condens. Matter* **12**, R207 (2000), and references therein.
 - [19] G. Ge and L. Brus, *J. Phys. Chem. B* **104**, 9573 (2000).
 - [20] U. Thiele, M. Mertig, and W. Pompe, *Phys. Rev. Lett.* **80**, 2869 (1998).
 - [21] J. N. Israelachvili, *Intermolecular and Surface Forces* (Academic, New York, 1992), 2nd ed.; B. A. Korgel and D. Fitzmaurice, *Phys. Rev. Lett.* **80**, 3531 (1998).
 - [22] Assuming that the surface is chemically homogeneous. See K. Kargupta *et al.*, *Langmuir* **17**, 1294 (2001).
 - [23] X. M. Lin *et al.*, *J. Phys. Chem. B* **105**, 3353 (2001).